The mobility of Mo during microbially-mediated ferrihydrite phase transformation

JING ZHANG [a b c], MENGQIANG ZHU [d], JONATHAN R. LLOYD [b], SAMUEL SHAW [b], VICTORIA S. COKER [b], JINXIN XIE [b], KE WEN [e], SUNGSIK LEE [f], THOMAS L. GOÛT [a], JINGYUE HAO [c], LIN MA [c], YANDI HU [a g*], & BO PAN [g h]*

[a] The Key Laboratory of Water and Sediment Sciences, Ministry of Education, State Environmental Protection Key Laboratory of All Material Fluxes in River Ecosystems, College of Environmental Sciences and Engineering, Peking University, Beijing 100871, China.

[b] Williamson Research Centre for Molecular Environmental Science, Department of Earth and Environmental Sciences, The University of Manchester, Manchester M13 9PL, U.K.

[c] Department of Chemical Engineering, The University of Manchester, Manchester M13 9PL, U.K.

[d] Department of Geology, University of Maryland, College Park, Maryland 20742, USA.

[e] Department of Ecosystem Science and Management, University of Wyoming, Laramie, Wyoming 82071, USA.

[f] X-ray Science Division, Argonne National Laboratory, Lemont, IL 60439, USA.

[g] Southwest United Graduate School, Kunming 650092, China.

[h] Yunnan Provincial Key Laboratory of Soil Carbon Sequestration and Pollution Control, College of Environmental Science & Engineering, Kunming University of Science & Technology, Kunming 650500, China.

***To Whom Correspondence Should Be Addressed**

E-mail: huyandi@pku.edu.cn

lin.ma@manchester.ac.uk

Submitted to:

Environmental Science & Technology

2024

TABLE OF CONTENTS FIGURE

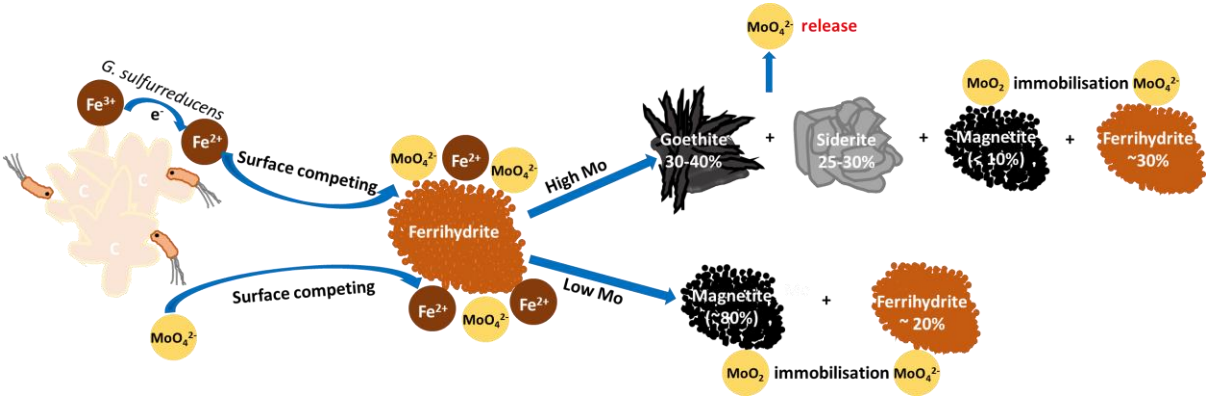

ABSTRACT

Molybdenum (Mo) is an essential nutrient for almost all organisms. However, at high concentrations, it can be toxic to animals and plants. This study investigated the interactions of Mo(VI) with iron oxyhydroxides during ferrihydrite bioreduction in the presence of the Fe(III)-reducing *Geobacter sulfurreducens*. Here we showed that Mo concentration controlled ferrihydrite phase transformation, leading to Mo release. With the biotic reduction of ferrihydrite and Fe(II) production, Mo(VI) reduction and Mo(IV)O_2 formation were observed for the first time, which further immobilised Mo after surface adsorption of Mo(VI). At low Mo levels (Mo/Fe molar ratios of 1-2 %), sufficient Fe(II) adsorption onto ferrihydrite resulted in its transformation into magnetite nanoparticles (>80%, ~25 nm) which catalysed the reduction of Mo(VI) to form Mo(IV)O_2 and immobilised Mo. Contrastingly, at high Mo concentrations (Mo/Fe molar ratios of 5-10%), Mo(VI)O_4^{2-} adsorption onto ferrihydrite limited Fe(II) adsorption, subsequently less magnetite (<8-12%) formed while more goethite (~30-50%, width & length > 15 & 100 nm, respectively) and siderite (~20-30%, width & length > 100 & 200 nm, respectively) with larger particle sizes formed instead, causing Mo(VI) release due to lower Mo adsorption. This study provides a comprehensive understanding of the interaction mechanisms among *Geobacter sulfurreducens*, Mo(VI), and iron oxyhydroxides, enabling predictions and controls of long-term Mo mobility and Fe mineral transformation under a variety of biogeochemical scenarios.

KEYWORDS: Molybdenum immobilisation, *Geobacter sulfurreducens,* ferrihydrite transformation, Mo(IV)O_2, Mo(VI) and Fe(II) competitive adsorption

SYNOPSIS: This study fills the information gap of interactions of Mo(VI)-ferrihydrite-*Geobacter sulfurreducens* ternary systems. Mo concentration controls ferrihydrite phase transformation, which controls Mo mobility in biogeochemical scenarios.

INTRODUCTION

Molybdenum (Mo) is an essential nutrient in biological systems [1-5], catalysing the global biogeochemical C, N, and S cycles and other important redox processes [1, 2, 6-8]. Mo normally exists as highly soluble tetrahedrally-coordinated molybdate ($Mo(VI)O_4^{2-}$), which can be reduced biologically (e.g. Mo-reduction bacteria) or abiotically (e.g. euxinic (sulphidic) environments) to insoluble octahedrally-coordinated $Mo(IV)O_2$ [9-11]. The changes in solubility of Mo(VI) to Mo(IV) underscore the significance of this study to understand the mobility of Mo in biogeochemical redox-active systems.

Mo is found in residues from industrial processes, such as mine wastes [12], and can also be released from minerals (*e.g.* molybdenite) through oxidative weathering, which can result in Mo in surface and groundwaters exceeding 900 ppm [1, 8, 11, 13]. Such high Mo concentrations can detrimentally affect environmental systems, such as by causing chlorosis in plants or molybdenosis in ruminants [1, 12, 14-16] and adverse reactions in microorganisms (*e.g.* Mo > 61 ppm for green algae) due to the importance of molybdoenzymes in cellular metabolism [12, 17]. However, the impacts of high concentrations of Mo, such as in contaminated environments, on bacteria remain unclear.

Iron oxides are ubiquitous in nature and represent a potential control on Mo mobility through adsorption [9, 18-29] and phase transformation in the presence of Fe(II) [30-36]. With low and high adsorbed amounts of Fe(II) on ferrihydrite, goethite and magnetite have been reported as the transformation products of ferrihydrite, respectively [31, 37-39]. In abiotic Mo(VI)-ferrihydrite-Fe(II) systems, Fe oxyhydroxides were reported to transform to goethite and lepidocrocite without the reduction of Mo(VI) to Mo(IV), which may due to the low concentration of Fe(II) [4, 31-33]. The biogenic redox cycling of Fe oxyhydroxides was studied using the dissimilatory metal-reducing bacterium, *Geobacter sulfurreducens* [40], which can reduce ferrihydrite ($Fe(III)(OH)_3$) to Fe(II) and form magnetite ($Fe(II)Fe(III)_2O_4$) [39, 41-49]. Further, the concentrations of anions could alter ferrihydrite phase transformation, as a previous study on V(V)-ferrihydrite-*G. sulfurreducens* reported goethite formation for samples with high V(V) concentration, and magnetite formation with low V(V) concentration [49]. However, the

underpinning mechanisms are unclear. The varied mineral transformation pathways reported in these systems indicate important interactions between Mo(VI), ferrihydrite, and *G. sulfurreducens*.

Here, we studied the Mo(VI)-ferrihydrite-*G. sulfurreducens* ternary system under varied Mo concentrations, aiming to understand the mechanisms of biotic-induced ferrihydrite phase transformation and its control on Mo(VI) mobility. We hypothesised that Mo concentration could control biotic-induced ferrihydrite phase transformation, either through concentration-dependent adverse effects on bacteria or competitive adsorption with Fe(II); mineral transformation, in turn, could control the reduction and mobility of Mo. Such understandings can be used to predict the long-term stability of Fe oxyhydroxides and Mo sequestration.

METHODS

Production of Mo(VI)-adsorbed ferrihydrite. Ferrihydrite was synthesised by neutralising a 0.4 M $FeCl_3$ solution using 10 M NaOH and washing the resulting solid in deionised water six times by centrifugation to removal residual ions [50]. To form Mo(VI)-adsorbed ferrihydrite, an experiment was performed by mixing washed ferrihydrite (10 mM as Fe), sodium acetate (10 mM), sodium bicarbonate (10 mM, as a pH buffer), and sodium molybdate ($Na_2Mo(VI)O_4 \bullet 2H_2O$; 0.1, 0.2, 0.5, and 1.0 mM) to obtain suspensions with Mo/Fe molar ratios of 1, 2, 5, and 10%. Previous work reported that the concentration of Mo in groundwater can reach 25 ppm [12] and the tolerance of Mo for some freshwater organisms can be over 61 ppm [17]. Therefore, it is of environmental relevance to study Mo concentration from 0.1 mM (~10 ppm) to 1.0 mM (~100 ppm), resulting in ratios of Mo and Fe of 1-10%, to investigate the effect of Mo concentration on microorganism activities and mineral phase transformation. Suspensions (pH 7) were degassed through sparging with N_2-CO_2 (80:20) gas and sealed in anaerobic bottles for five days (counted as Day -5 to Day 0).

Metal reduction by *Geobacter sulfurreducens*. *Geobacter sulfurreducens* were obtained from the laboratory culture collection of the Geomicrobiology Group in the Department of Earth and Environmental Sciences, University of Manchester, UK. Cells were grown in modified fresh water medium under anaerobic conditions at 30 °C [42], with the addition of sodium acetate (20 mM) as the electron donor and sodium fumarate (40 mM) as the electron acceptor. All manipulations were performed in an anaerobic chamber (95% N_2 / 5% H_2) or under N_2-CO_2 (80:20) gas to provide O_2-free conditions. *G. sulfurreducens* were harvested at late-log phase by centrifuging at 4960 *g* for 20 minutes at 4 °C, and then washed twice using 30 mM

bicarbonate buffer ($NaHCO_3$) under an atmosphere of N_2-CO_2 (80:20). The optical density (OD_{600}) was measured to determine the concentration of bacteria by UV-vis spectrophotometry (Jenway 6715 series) at 600 nm. *G. sulfurreducens* (OD_{600}=0.4) were added to Mo(VI)-Fe oxyhydroxide suspensions and incubated at 30 °C.

Bacteria addition to the system was defined as Day 0, and experiments lasted until Day 12. Comparison experiments were performed by mixing *G. sulfurreducens* (OD_{600}=0.4) with aqueous Mo(VI) (0.1, 0.2, 0.5, and 1.0 mM) without the addition of ferrihydrite for 5 days to study the direct bacterial adsorption and redox capacity of *G. sulfurreducens* for Mo, as well as the toxicity of Mo to *G. sulfurreducens* [11, 51]. Blank experiments were conducted by mixing ferrihydrite with *G. sulfurreducens* without the addition of Mo to compare with bio-induced mineral phase transformation. Additional abiotic experiments of Mo(VI)-magnetite and Mo(VI)-Fe(II) (1% Mo, 10 mM Fe(II), pH 7) binary systems and a Mo(VI)-Fe(II)-ferrihydrite (1 and 10% Mo, 10 mM Fe(II) and Fe(III), pH 7) ternary system were performed to characterise Mo(VI) reduction and ferrihydrite phase transformation.

Analytical techniques. After different time intervals (from day -5 to 12), suspensions were centrifuged. Concentrations of dissolved Mo and Fe in solution were measured using inductively coupled plasma mass spectrometry (ICP-MS) (PerkinElmer Optima 5300 dual view) by filtering and acidifying supernatant using 0.22 μm filters and 2% HNO_3, respectively. Fe(II) concentration (mmole Fe(II) per litre of slurry) was monitored using the Ferrozine assay by combining the slurry (a mixture of solution and solid) with 0.5 M HCl for 1 hour [45, 47, 52-54]. This protocol can extract Fe(II) that is sorbed or extractable from reasonably labile Fe minerals (e.g. siderite). The concentration of aqueous Fe(II) in the supernatants was also measured and results showed no aqueous Fe(II) was detected. The concentration of Mo in solution decreased between Days 1-4 and then increased after Day 5. Therefore, solid samples were taken on Day 5 after the addition of bacteria for further characterisation (XRD, ATR-FTIR, TEM, and XAS) to better understand the Mo concentration change in solution. Samples were prepared in a glove box (95% N_2 / 5% H_2) and were taken out and measured immediately for analysis, using sealed containers equilibrated with the glovebox atmosphere to facilitate sample transport.

Powder X-ray diffraction (XRD, Bruker D8 Advance Diffractometer) and attenuated total reflectance-Fourier transform infrared spectroscopy (ATR-FTIR, Shimadzu IRTracer-100) were performed on samples with Mo/Fe molar ratios of 1, 2, 5, and 10% after 5 days of incubation with bacterial cells. XRD was also conducted for abiotic samples of 1% and 10% in the Mo(VI)-ferrihydrite-Fe(II) ternary system with an Fe(II):Fe(III) ratio of 1. Crystallite

sizes of newly formed sphere-shaped minerals were calculated by comparing the full width at half maximum (FWHM) using the Scherrer equation (Eq. 1) [55, 56].

$$D_{hkl} = \frac{K\lambda}{B_{hkl} \cos \theta} \quad (1)$$

where: D_{hkl} is the crystallite size of the ordered domains; K is the crystallite-shape factor (0.9); λ is the X-ray wavelength; B_{hkl} is the FWHM of the XRD peaks after subtracting the instrumental broadening in radians; and θ is the Bragg angle [55, 56].

Transmission electron microscopy (TEM, FEI Tecnai G2 F20) was carried out to image the morphology of solid samples with 1% and 10% Mo after 5 days incubation with bacterial cells, as well as for the samples from an abiotic experiment of 1% Mo(VI)-ferrihydrite-Fe(II) with an Fe(II):Fe(III) ratio of 1. Particles were washed twice to remove buffer solution and cells. Sample suspensions were dropped onto holey carbon coated copper grids before introduction to the microscope. Energy dispersive spectroscopy (EDS) and selected area electron diffraction (SAED) were also performed. Further details regarding data analysis of the SAED patterns are given in the supporting information (Text S1).

X-ray Absorption Spectroscopy (XAS) analyses were conducted on Mo(VI)-Fe oxyhydroxide samples at 1-10% Mo after 5 days incubation with bacterial cells. X-ray Absorption Near Edge Structure (XANES) and Extended X-ray Absorption Fine Structure (EXAFS) data were collected on beamline 12-BM at Advanced Photon Source (APS) and BL4-1 at Stanford Synchrotron Radiation Lightsource (SSRL), U.S., at the Mo (20 keV) and Fe (7.112 keV) K-edge in fluorescence mode. Solid particles were pelleted and mounted to sample holder plates using Kapton tape. Spectra collected at SSRL and APS used Si(220) and Si(111) monochromators, respectively. Reference standards for Mo (molybdenum dioxide ($Mo(IV)O_2$), sodium molybdate ($Na_2Mo(VI)O_4 \cdot 2H_2O$), bamfordite ($FeMo(VI)_2O_6(OH_3) \cdot H_2O$), and heptamolybdate ($(NH_4)_6Mo(VI)_7O_{24}$)) and Fe (ferrihydrite, goethite, siderite, and magnetite) were prepared by diluting standard powders with cellulose to make pellets for XAS data collection at Mo and Fe K-edge, respectively, in transmission mode at room temperature. Additionally, Mo(VI)-adsorbed ferrihydrite/goethite/magnetite reference materials were measured at Mo K-edge in fluorescence mode. Mo-incorporated goethite was cited from a previous publication [20] for linear combination fitting (LCF) to determine if Mo was incorporated into the goethite structure. Data analyses, including background subtraction, normalisation, and calibration, were performed using Athena and Artemis [37]. Further details on the preparation of the reference materials, Mo and Fe K-edge XANES and EXAFS LCF

(including estimated errors), and Mo EXAFS shell-by-shell fitting are presented in the supporting information (Text S2&S3, Figure S8, & Table S2).

RESULTS AND DISCUSSION

Ferrihydrite reduction and Mo(IV)O_2 formation. During abiotic adsorption (Figure 1a), rapid Mo adsorption onto ferrihydrite removed aqueous Mo to ~0.03-0.05 mM and ~0.2-0.5 mM for samples with low (1% and 2%) and high (5% and 10%) initial Mo concentrations, respectively, and these values remained stable from Day -5 to -1. This is consistent with Ferrozine results (Figure 1b) where no Fe(II) was detected, indicating fast adsorption of Mo(VI) rather than reduction to Mo(IV) occurred at Step I.

After adding *G. sulfurreducens* (Day 0), the concentration of Mo in solution further decreased to 0.1-0.3 mM and only ~0.01 mM for systems with high and low Mo concentrations by Day 4 (Step II, Figure 1a), respectively. After Day 4 (Step III), for experiments with high Mo, the amount of Mo in solution began to increase to 0.2-0.5 mM by Day 12 (Step III, Figure 1a), while such increase was negligible for the low Mo experiments.

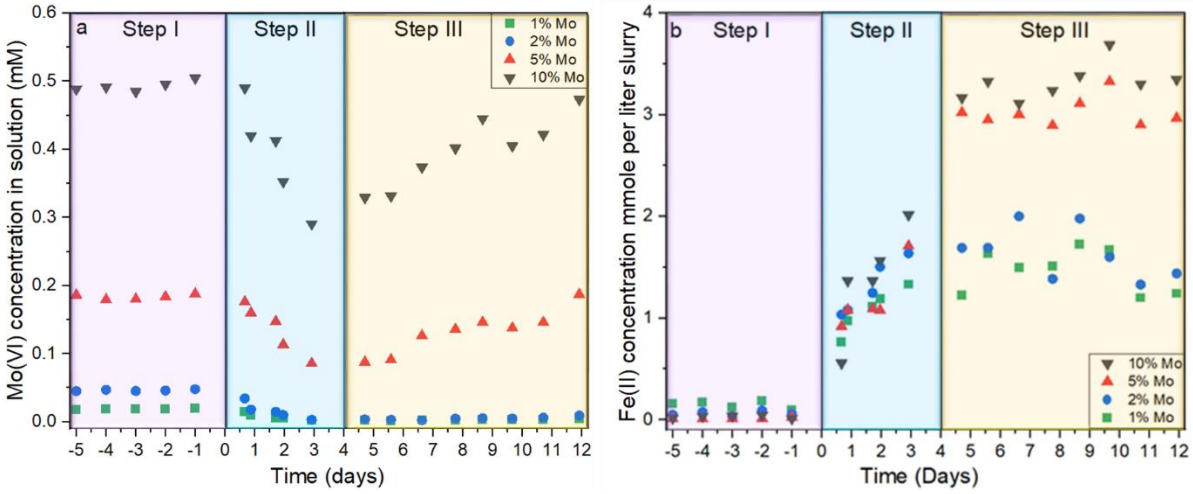

Figure 1 Mo(VI) (a) concentration in solution and Fe(II) (b) concentration per litre slurry during abiotic adsorption onto ferrihydrite (Step I, Day -5 to -1) and bio-induced transformation at Day 0 to 12 (Step II: decreasing Mo(VI) concentration due to its reduction to Mo(IV) to form Mo(IV)O_2 and increasing Fe(II) concentrations from the reduction of Fe(III) at Day 0 to 4; Step III: Mo(VI) release into solution and further Fe(II) increase in the slurry at high Mo concentrations (5% and 10%), and Mo immobilisation and stable Fe(II) levels in the slurry at low Mo concentrations (1% and 2%) at Day 5 to 12).

The decreasing concentration of Mo(VI) in solution after the addition of *G. sulfurreducens* in Step II may be related to three processes: (1) Mo adsorption/uptake by bacteria, (2) Mo(VI) reduction to form insoluble $Mo(IV)O_2$ [57, 58], and/or (3) bio-induced coprecipitation of Mo and Fe. However, a comparison experiment with *G. sulfurreducens* and Mo (0.1-1 mM) without ferrihydrite showed no concentration change of Mo(VI) in solution over 5 days of incubation (Figure S1 in supporting information), indicating that the decrease in concentration of Mo(VI) in solution during Step II was not due to Mo adsorption/uptake by *G. sulfurreducens,* excluding the first hypothesis.

The decreasing Mo(VI) levels in solution may be due to the reduction of Mo(VI) to form $Mo(IV)O_2$, which has a lower solubility. TEM-EDS showed the formation of $Mo(IV)O_2$ precipitates, with substantial Mo enrichment alongside Fe depletion (Figure 2b, c) in the red rectangular area in Figure 2a. Interplanar spacings were measured (0.32 nm, Figure 2d), consistent with a previous study which indicated a (-111) crystallographic plane of monoclinic MoO_2 [59]. The corresponding selected area electron diffraction (SAED, Figure 2e) identified the (-101), (200), (-212), and (-321) planes of monoclinic MoO_2 (JCPDS card no.32-0671), proving the second hypothesis.

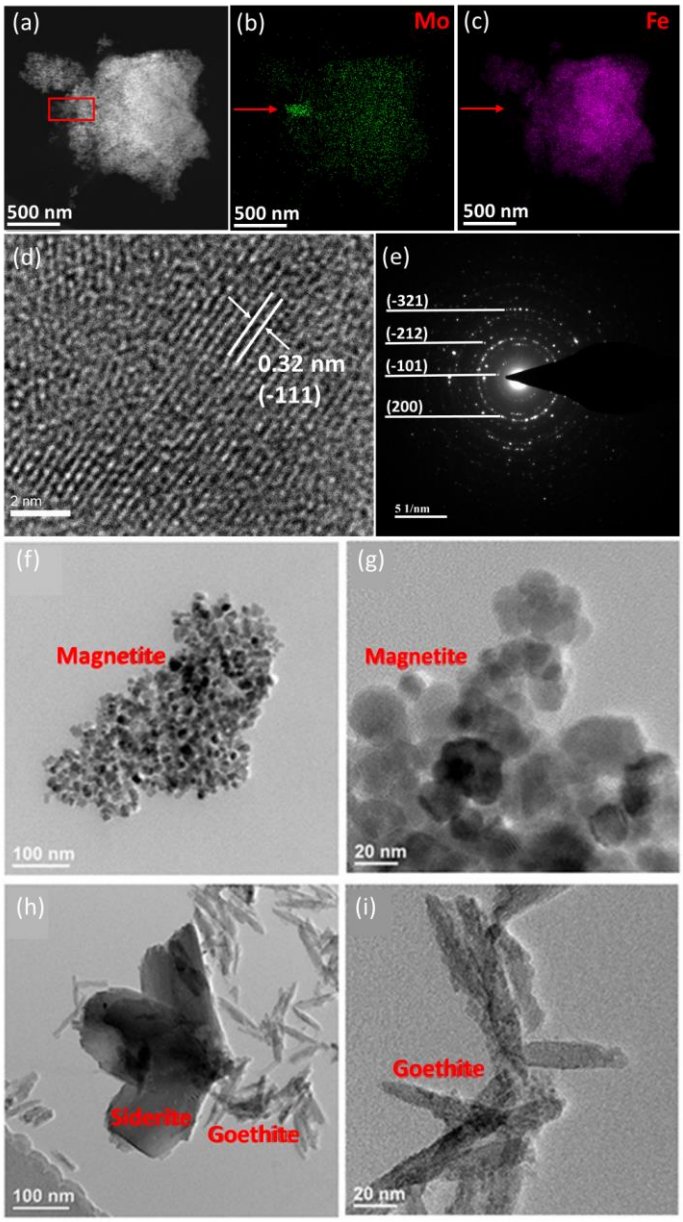

Figure 2 TEM of Fe oxyhydroxides formed in 1% and 10% Mo solutions after bacteria addition at Day 5. EDS elemental mapping images for the sample with 1% Mo from the selected region (a) for Mo (b) and Fe (c). HRTEM image (d) and SAED pattern of MoO_2 (e). TEM images for the sample with 1% Mo (f and g (zoomed in)) and 10% Mo (h and i (zoomed in)).

XANES data (Figure 3) were consistent with the TEM results (Figure 2). As XANES at the Mo K-edge (Figure 3a) showed, all samples at Day 5 displayed weaker intensities for the pre-edge peaks (20004 eV) than the starting material ($Na_2Mo(VI)O_4 \cdot 2H_2O$ tetrahedral compounds), better corresponding to the Mo(IV) reference standard that lacks a pre-edge peak. The strong pre-edge transition in the Mo(VI) reference arises from overlap between the vacant 4d and 5p states owing to the lack of inversion/centrosymmetry in the Mo tetrahedron, while the Mo(IV)

reference, which is octahedral with comparatively higher symmetry, has a small pre-edge feature that is smoothed out due to broadening effects in the spectrum [60]. The pre-peak intensity of the samples indicated $Mo(VI)O_4^{2-}$ may reduce to Mo(IV) in the solid [9].

The relative proportions of Mo(IV) were quantified through linear combination fitting. XANES LCF (Figure S2a & Table S1) showed that over 50% of the total Mo in the solid can be represented by $Mo(IV)O_2$ for samples at low Mo levels (1% and 2%) and less than 30% for samples with high Mo levels (5% and 10%). For samples with high Mo concentrations (5% and 10%), EXAFS LCF (Figure S2c& Table S1) showed good fittings, and the results were consistent with XANES LCF (Figure S2a & Table S1) that 20-30% Mo(VI) was reduced to Mo(IV). For samples with low Mo levels (1% and 2%), although EXAFS LCF did not adequately fit the data (i.e., misfits at k = 5.5-8 $Å^{-1}$, indicating the existence of some potential unknown species), these results remained consistent with those of the XANES LCF, which showed that over 50% Mo(VI) was reduced to Mo(IV). Both XANES and EXAFS LCF further confirmed the TEM-EDS/SAED result that Mo(VI) was reduced to Mo(IV) and formed $Mo(IV)O_2$.

A previous abiotic study reported the formation of bamfordite ($Fe(III)Mo(VI)_2O_6(OH_3)•H_2O$) in the Mo(VI)-ferrihydrite-Fe(II) system [4]. The coprecipitation of Mo with Fe to form new minerals, such as bamfordite, could lead to a decrease of Mo(VI) in solution. However, the LCF result (Table S1) indicated no bamfordite formation in our biotic system (Mo(VI)-ferrihydrite-*G. sulfurreducens*), excluding the third possibility.

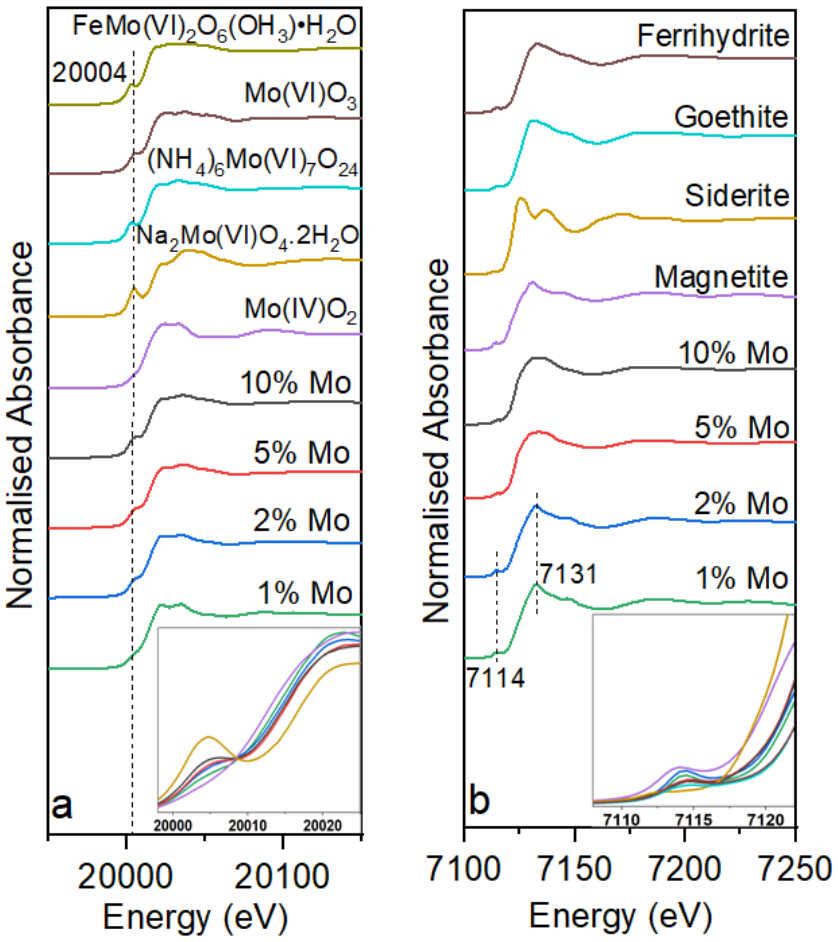

Figure 3 Mo (a) and Fe (b) K-edge XANES (inserts are zoomed-in figures of the pre-edge region) show Mo(VI) reduction (a) and ferrihydrite transformation (b) for samples with 1-10 % Mo at Day 5. Reference standards for Mo ($Mo(IV)O_2$, $Na_2Mo(VI)O_4{\cdot}2H_2O$, $(NH_4)_6Mo(VI)_7O_{24}$, $Mo(VI)O_3$, and $FeMo(VI)_2O_6(OH_3){\cdot}H_2O$) and Fe (magnetite, siderite, goethite, and ferrihydrite) are also presented in (a) and (b), respectively.

In summary, following Mo adsorption onto ferrihydrite, further Mo concentration decrease was observed after the addition of bacteria, which was found to be due to Mo(VI) reduction and the formation of insoluble $Mo(IV)O_2$. To understand the mechanism, two comparison experiments with Mo(VI)-*G. sulfurreducens* and Mo(VI)-Fe(II) binary systems were conducted. These results showed no changes in the concentration of aqueous Mo(VI) (Figure S1), demonstrating that *G. sulfurreducens* or Fe(II) alone was not able to reduce Mo(VI) to form $Mo(IV)O_2$ in the absence of ferrihydrite and indicating potential effects of newly formed Fe oxide phases from ferrihydrite transformation. The following two subsections will discuss ferrihydrite phase transformation controlled by Mo concentration, and the reduction of Mo(VI) to $Mo(IV)O_2$ by newly formed Fe oxide phases.

Mo concentrations control ferrihydrite phase transformation. After the addition of bacteria, the production of Fe(II) suggested ferrihydrite reduction and mineral transformation occurred (Figure 1b, Step II and III). Products of the mineral phase transformation were observed to depend on the initial concentration of Mo(VI) by multiple techniques including XRD, FTIR, TEM, and XANES.

XRD (Figure 4) was performed on samples taken on Day 5 after incubation with *G. sulfurreducens*: at low Mo levels (1% and 2%), ferrihydrite transformed to magnetite; while at high Mo concentration (5% and 10%), goethite and siderite formed. A similar observation was reported in a previous study on ferrihydrite biogenic transformation in the presence of V(V) and *G. sulfurreducens*, that also observed magnetite at low levels, and goethite and siderite at high concentrations [49]. However, the controlling mechanisms for different transformation pathways of ferrihydrite were unexplored. For experiments without the addition of *G. sulfurreducens* (Figure 4, NC), no transformation was observed in the Mo(VI)-ferrihydrite binary system; while for experiment without the addition of Mo(VI) (Figure 4, 0% Mo), ferrihydrite transformed to magnetite in the ferrihydrite-*G. sulfurreducens* binary system, consistent with previous studies that *G. sulfurreducens* can induce ferrihydrite transformation to magnetite [39, 44, 61].

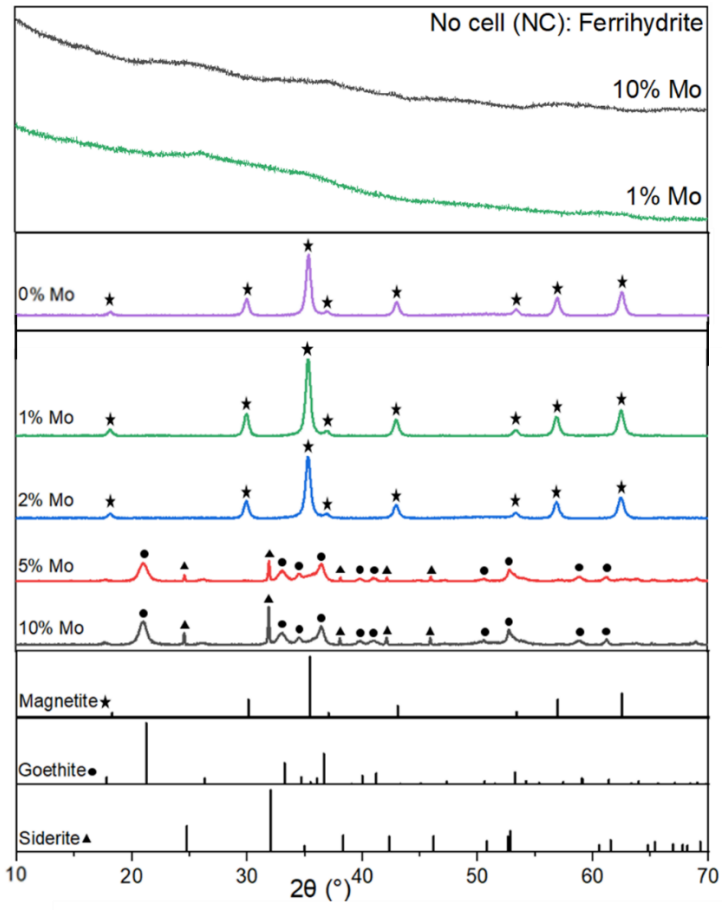

Figure 4 XRD patterns for ferrihydrite samples with 0% - 10% Mo and cell on Day 5 and comparison experiments with 1% and 10% Mo-ferrihydrite samples without cell (NC).

At high Mo levels (5% and 10%), a wide and intense peak at ~1411 cm^{-1} and a small peak at ~864 cm^{-1} were observed by FTIR (Figure S3a), similar to reported siderite characteristic spectra [62]. Further, a peak observed at ~790 cm^{-1} was consistent with that of the goethite standard measured here. For samples with a low initial Mo concentration (1% and 2%), two peaks at 1500-1700 cm^{-1} were observed, corresponding to the magnetite standard. For experiments without *G. sulfurreducens*, spectra for samples in all systems were similar to ferrihydrite, indicating no phase transformation without bacteria (Figure S3b).

Mineral morphologies were determined by TEM (Figure 2f, g, h, i): needle-shaped goethite crystals with lengths over 100 nm were dominant in the sample containing 10% Mo (Figure 2h&i), which were similar to experiments carried out previously on the biotransformation of V(V)- or Sb(V)-bearing ferrihydrite [45, 49]. The 10% Mo sample also contained platy-minerals with a width and length over 100 nm and 200 nm, respectively, consistent with the formation of Fe carbonate (siderite) as identified by XRD (Figure 4). For the 1% Mo sample, nanosized,

spherical particles (~25 nm) were observed (Figure 2f&g), corresponding to magnetite formation (Figure 4) [45].

Fe K-edge XANES spectra and LCF also showed consistent mineral phases (Figure 3b, S2b, & S2d, & Table S1). For samples with an initial low Mo concentration (1% and 2%) at Day 5, Fe XANES (Figure 3b) contained a pre-edge peak at ~7114 eV and a sharp peak at ~7131 eV, consistent with the magnetite reference standard which is a mixture of Fe(II) and Fe(III) [63]. For samples with high Mo concentration (5% and 10%), the pre-edge peak diminished and became similar to the goethite reference standard (pure Fe(III) mineral), but the overall structure did not precisely match any of these reference standards, indicating the potential formation of a mixture of minerals. Therefore, LCF (Table S1) was used to quantify the relative abundance of the Fe oxide phases. Both XANES and EXAFS LCF showed that magnetite accounted for over 80% of total Fe mineral for samples with low concentrations of Mo (1% and 2%). However, only less than 8-12% magnetite was fitted for samples with high Mo concentrations (5% and 10%), and instead goethite (~30-50%) and siderite (~20-30%) dominated (Table S1 & Figure S2).

Previous studies have reported both abiotic and biotic Fe(II)-catalysed ferrihydrite transformation to magnetite, and sufficiently high Fe(II) surface adsorption onto ferrihydrite is identified as a key step leading to magnetite formation [31, 37-39]. Hansel *et al*. studied ferrihydrite transformation under two Fe(II) concentrations, and found that magnetite can form with $[Fe(II)]_{mol}$:$[Fe(III)]_{mol}$ = 1:6 [37], while goethite/lepidocrocite formed with $[Fe(II)]_{mol}$:$[Fe(III)]_{mol}$ = 1:60. The formation of magnetite at no/low Mo concentration in our systems is attributed to the microbially-induced reductive dissolution of Fe(III)-oxyhydroxide in these experiments: *G. sulfurreducens* attached to the ferrihydrite surface and subsequently induced Fe(III) dissolution and reduction to Fe(II) [39, 49, 53]. The reduced Fe(II) then adsorbed onto ferrihydrite, leading to magnetite formation [39].

As the formation of magnetite depends on the concentration of adsorbed Fe(II) on the ferrihydrite surface [37-39], we first hypothesised that the different mineral transformation products (*i.e.*, goethite and siderite instead of magnetite) at high Mo concentrations could be due to inhibited Fe(II) production through toxic effects of Mo on microbial activities. To test the first possibility, the concentration of Fe(II), which was produced by bacterial induced Fe(III) reduction, was checked. However, Fe XANES and EXAFS LCF (Table S1) showed the amounts of Fe(II) were similar for samples with both low and high Mo concentrations, *i.e.*, 26-27% and 22-32%, respectively. This agreed with data for *G. sulfurreducens* growth over a wide

Mo concentration range (0.1-1 mM) without ferrihydrite addition (Figure S4), which showed a negligible impact of high Mo concentration on the growth of *G. sulfurreducens,* different from previous reports that Mo concentrations (> 61ppm) can have adverse reactions with green algae [12, 17], excluding the first possibility.

Subsequently, we hypothesised that inhibited Fe(II) adsorption onto ferrihydrite could occur at high Mo(VI) concentration. Schoepfer *et al.* studied the Mo(VI)-ferrihydrite-Fe(II) ternary system with varied Mo(VI) concentrations (0-100 μmol/g) but did not observe magnetite formation [4]. We postulate the insufficient Fe(II) addition ($[Fe(II)]_{mol}$:$[Fe(III)]_{mol}$ = 1:400) in their study limited ferrihydrite transformation into magnetite. Coker *et al.* studied the V(V)-ferrihydrite-bacteria ternary system, and reported similar magnetite formation with low V concentrations (0-4.2 %) and goethite formation at high V concentration (7.4 %) [49]. However, the mechanisms underpinning how V(V) concentrations could control ferrihydrite transformation were not discussed. Here, we hypothesised that the limited available surface sites for Fe(II) adsorption for samples with high Mo/V concentrations led to ferrihydrite transformation to goethite, instead of magnetite. To test this, experiments of Mo(VI)-ferrihydrite-Fe(II) with high Fe(II) ($[Fe(II)]_{mol}$:$[Fe(III)]_{mol}$ = 1) and different Mo levels (1% and 10%) were performed, and XRD demonstrated the formation of magnetite and goethite with low and high Mo levels, respectively (Figure S5).

To summarise, at high Mo concentrations, substantial amounts of Mo(VI) remained in solution (~40-50%, Figure 1a, Step II), which we postulate led to a significant decrease in Fe(II) adsorption on ferrihydrite through competition for surface sites. This would hinder the formation of magnetite at high Mo concentrations and caused the production of goethite and siderite [31, 37]. The direct observation of competitive adsorption of Mo and Fe onto ferrihydrite and the corresponding molecular-scale mechanisms require further investigation. For samples at low Mo concentration, sufficient available surface sites for Fe(II) adsorption facilitated magnetite production. The formation of siderite may be attributed to the reaction of free bio-reduced Fe(II) with carbonate in the buffer solution [45].

Mineral phase transformation controls Mo mobility and Fe(II) production. As discussed in the first subsection, the rapid adsorption of Mo(VI) caused the decrease in aqueous Mo(VI) (Step I, Figure 1a), followed by the reduction of Mo(VI) to Mo(IV) to form $Mo(IV)O_2$ precipitates leading to the further decrease of Mo(VI) in solution (Step II, Figure 1a). Interestingly, Mo in solution increased after Day 5 in Step III for samples with high initial Mo concentrations (5% and 10%), while negligible changes occurred for samples with low initial

Mo concentrations (1% and 2%). In this subsection, two processes related to the different Fe oxide phase transformation in step III, which could cause Mo release/immobilisation, will be discussed to elucidate this phenomenon: (1) Mo(VI) adsorption onto newly formed Fe oxide minerals, and (2) reduction of Mo(VI) by newly formed Fe oxide minerals to form insoluble $Mo(IV)O_2$.

Firstly, particle sizes of newly formed Fe oxide minerals, which could affect Mo(VI) adsorption, were semi-quantitatively determined by TEM, which showed needle-shaped goethite crystals with a width and length over 15 nm and 100 nm, respectively, and platy-shaped siderite with a width and length over 100 nm and 200 nm, respectively, for the sample containing 10% Mo (Figure 2h&i). Contrastingly, for the 1% Mo sample, spherical magnetite nanoparticles (diameter ~25 nm) were observed under TEM, consistent with the calculated crystallite size (~28 nm) using Scherrer equation based on XRD measurements [55, 56]. As particle sizes of mineral transformation products all exceeded that of the initial ferrihydrite phase (diameter <10 nm) [63, 64], Mo desorption is postulated to cause the release of Mo back into the solution from Day 5 to 12, with this effect more pronounced for samples with initial high Mo concentrations (Figure 1a, Step III). Indeed, magnetite and goethite were reported to have similar/slightly lower adsorption capacity than ferrihydrite [30, 65, 66], while large siderite crystals with much lower surface area could have a much lower adsorption capacity for Mo(VI).

Secondly, different capabilities of the newly formed Fe oxide phase to reduce Mo(VI) and form $Mo(IV)O_2$ were considered. As more MoO_2 was produced in samples with more magnetite formation (*i.e.*, samples with low initial Mo concentrations, Table S1), we hypothesised that magnetite could reduce Mo(VI) to $Mo(IV)O_2$. This was proven by an additional experiment of Mo(VI) interaction with magnetite: 55.8% Mo(VI) was reduced to $Mo(IV)O_2$ by magnetite according to Mo K-edge XANES LCF (Figure S6). A previous abiotic study of Mo(VI)-ferrihydrite-Fe(II) showed no Mo(VI) reduction to Mo(IV) and no magnetite formation [4]. We postulate that the low Fe(II) concentration used in their study limited magnetite formation and thus no Mo(VI) reduction occurred, implying the important role of magnetite in Mo(VI) reduction. Our hypothesis was further validated by an abiotic experiment of Mo(VI)-ferrihydrite-Fe(II) with high Fe(II) (Fe(II):Fe(III) = 1) and low Mo (1%) levels, with magnetite formation (Figure S5), MoO_2 was observed by TEM-EDS: interplanar spacings from HRTEM images (0.24 nm, Figure S7a) and the corresponding SAED pattern (Figure S7b) were indexed as the (-202), (310), (-213), (210) planes of monoclinic MoO_2 (JCPDS card no.32-0671).

It has been demonstrated that the structural Fe(II) in magnetite is a strong electron donor [67-70], and magnetite has been reported to reduce several heavy metals, including hexavalent chromium Cr(VI) and hexavalent uranium U(VI) [69]. Therefore, we assume that structural Fe(II) in magnetite could reduce Mo(VI) to Mo(IV). The oxidised product of magnetite was not detected here, which could be explained by two possibilities. Firstly, maghemite, commonly reported as the oxidised product of magnetite, had similar diffraction patterns as magnetite [71]. So XRD and TEM/SEAD could not differentiate between them. Secondly, previous studies reported that dissimilatory iron reduction bacteria (DIRB) [72] could reduce ferric oxides and produce Fe(II), recovering the reducibility of magnetite through electron transfer from adsorbed Fe(II) to oxidised magnetite [69, 70]. Further investigation on the mechanisms of Mo(VI) reduction by magnetite could be an interesting future direction.

Concentrations of 0.5 M HCl extractable Fe(II) from slurry, including sorbed Fe(II) and Fe(II) in labile Fe minerals (e.g. siderite), also showed interesting trends. Extractable Fe(II) concentrations from slurry increased in all systems at Step II (Figure 1b), attributed to microbial-induced ferrihydrite reduction and the absorption of produced Fe(II) onto mineral surfaces. During Step III, for samples with low Mo concentrations, extractable Fe(II) concentration became stable, as the formation of magnetite (Figure 2&4, & Table S1) could turn more newly produced Fe(II) into non-extractable Fe(II). While for samples with high Mo levels, extractable Fe(II) concentration in slurry continued increasing, as the formed siderite could be dissolved by 0.5 M HCl within 1 hour.

ENVIRONMENTAL IMPLICATIONS

The release and immobilisation of Mo in biogeochemical systems is important for the environmental cycling of this key element as an important nutrient and contaminant. This study investigated Mo mobility and ferrihydrite phase transformation in the Mo(VI)-ferrihydrite-*G. sulfurreducens* ternary system. Competitive adsorption of Mo(VI) and Fe(II) onto ferrihydrite was found to control its phase transformation predominantly into magnetite (low initial [Mo]) or goethite/siderite (high initial [Mo]). In turn, sizes of the newly formed Fe oxide phases controlled Mo(VI) adsorption/desorption, and magnetite reduced Mo(VI) to $Mo(IV)O_2$ to immobilise Mo, while siderite formation released Mo. These new observations show that mineral phase transformation and Mo speciation changes with different initial Mo concentrations followed differing pathways, which control the mobility of Mo and bioavailability of Fe, representing a crucial factor governing the prolonged stability of Mo and Fe. This study highlighted the important role of Mo concentration in the biogeochemical cycle

of Mo and Fe, providing comprehensive insights for predicting and controlling the mobility and fate of heavy metals under a variety of biogeochemical scenarios.

SUPPORTING INFORMATION

Description of sample preparation and analysis of TEM and XAS; ICP-MS, OD_{600}, XRD, TEM, and FTIR data for blank and comparison experiments; results of XANES and EXAFS LCF and EXAFS shell-by shell fitting for the Mo(VI)-ferrihydrite-*G. sulfurreducens* system.

ACKNOWLEDGEMENTS

This work was supported by Yunnan Provincial Science and Technology Project at Southwest United Graduate School (202302AP370002), National Natural Science Foundation of China (No. 42177193), UMRI 2021-2022 Fund at University of Manchester, and NERC fellowship (NE/R013527/1). This research used resources of the Advanced Photon Source (beamline 12-BM), a U.S. Department of Energy (DOE) Office of Science user facility operated for the DOE Office of Science by Argonne National Laboratory under Contract No. DE-AC02-06CH11357. Use of the Stanford Synchrotron Radiation Lightsource (beamline 4-1), SLAC National Accelerator Laboratory, is supported by the U.S. Department of Energy, Office of Science, Office of Basic Energy Sciences under Contract No. DE-AC02-76SF00515. We thank Chuan Liu and John Waters for their help on XRD data analysis and Ryan Davis for the support on XAS data collection. We are also grateful to Ka Ki Wong for helping with sample shipping to Advanced Light Source (APS, USA).

REFERENCES

1. Smedley, P. L.; Kinniburgh, D. G., Molybdenum in natural waters: A review of occurrence, distributions and controls. *Applied Geochemistry* **2017,** *84*, 387-432.
2. Schwarz, G.; Mendel, R. R.; Ribbe, M. W., Molybdenum cofactors, enzymes and pathways. *Nature* **2009,** *460*, (7257), 839-847.
3. WHO *Molybdenum in drinking-water: background document for development of WHO guidelines for drinking-water quality*; World Health Organization: 2003.
4. Schoepfer, V. A.; Lum, J. E.; Lindsay, M. B. J., Molybdenum(VI) Sequestration Mechanisms During Iron(II)-Induced Ferrihydrite Transformation. *ACS Earth and Space Chemistry* **2021,** *5*, (8), 2094-2104.
5. Schoepfer, V. A.; Qin, K.; Robertson, J. M.; Das, S.; Lindsay, M. B. J., Structural Incorporation of Sorbed Molybdate during Iron(II)-Induced Transformation of Ferrihydrite and Goethite under Advective Flow Conditions. *ACS Earth and Space Chemistry* **2020,** *4*, (7), 1114-1126.
6. Wahl, B.; Reichmann, D.; Niks, D.; Krompholz, N.; Havemeyer, A.; Clement, B.; Messerschmidt, T.; Rothkegel, M.; Biester, H.; Hille, R., Biochemical and spectroscopic characterization of the human mitochondrial amidoxime reducing components hmARC-1 and

463 hmARC-2 suggests the existence of a new molybdenum enzyme family in eukaryotes. *Journal*
464 *of Biological Chemistry* **2010,** *285*, (48), 37847-37859.
465 7. Maia, L. B.; Moura, I.; Moura, J. J., Molybdenum and tungsten-containing enzymes:
466 an overview. In *Molybdenum and Tungsten Enzymes: Biochemistry*, The Royal Society of
467 Chemistry: 2016; pp 1-80.
468 8. Sheng, Y.; Baars, O.; Guo, D.; Whitham, J.; Srivastava, S.; Dong, H., Mineral-Bound
469 Trace Metals as Cofactors for Anaerobic Biological Nitrogen Fixation. *Environmental Science*
470 *& Technology* **2023,** *57*, (18), 7206-7216.
471 9. Zhang, J.; Coker, V. S.; Mosselmans, J. F. W.; Shaw, S., Adsorption of Octahedral
472 mono-molybdate and poly-molybdate Onto Hematite: A Multi-technique Approach. *Journal*
473 *of Hazardous Materials* **2022,** *431*, 128564.
474 10. Christiansen, T. L.; Bøjesen, E. D.; Juelsholt, M.; Etheridge, J.; Jensen, K. M., Size
475 induced structural changes in molybdenum oxide nanoparticles. *ACS nano* **2019,** *13*, (8), 8725-
476 8735.
477 11. Yakasai, H. M.; Rahman, M. F.; Manogaran, M.; Yasid, N. A.; Syed, M. A.; Shamaan,
478 N. A.; Shukor, M. Y., Microbiological reduction of molybdenum to molybdenum blue as a
479 sustainable remediation tool for molybdenum: a comprehensive review. *International journal*
480 *of environmental research and public health* **2021,** *18*, (11), 5731.
481 12. Barceloux, D. G.; Barceloux, D., Molybdenum. *Journal of Toxicology: Clinical*
482 *Toxicology* **1999,** *37*, (2), 231-237.
483 13. Guo, H.; Gao, Z.; Xing, S., Water–Rock Interactions: Mineral Dissolution. *Medical*
484 *Geology: En route to One Health* **2023**, 111-127.
485 14. Essilfie-Dughan, J.; Pickering, I. J.; Hendry, M. J.; George, G. N.; Kotzer, T.,
486 Molybdenum speciation in uranium mine tailings using X-ray absorption spectroscopy.
487 *Environmental science & technology* **2011,** *45*, (2), 455-460.
488 15. Das, A. K.; Chakraborty, R.; Cervera, M. L.; De la Guardia, M., A review on
489 molybdenum determination in solid geological samples. *Talanta* **2007,** *71*, (3), 987-1000.
490 16. Bassari, A., Radioisotope excited EDXRF analysis of sediment core samples from the
491 southern part of the Black Sea+. *Journal of Radioanalytical and Nuclear Chemistry* **2001,** *250*,
492 (1), 129-137.
493 17. De Schamphelaere, K.; Stubblefield, W.; Rodriguez, P.; Vleminckx, K.; Janssen, C.,
494 The chronic toxicity of molybdate to freshwater organisms. I. Generating reliable effects data.
495 *Science of the total environment* **2010,** *408*, (22), 5362-5371.
496 18. Xu, N.; Christodoulatos, C.; Braida, W., Adsorption of molybdate and
497 tetrathiomolybdate onto pyrite and goethite: effect of pH and competitive anions. *Chemosphere*
498 **2006,** *62*, (10), 1726-1735.
499 19. Arai, Y., X-ray Absorption Spectroscopic Investigation of Molybdenum Multinuclear
500 Sorption Mechanism at the Goethite− Water Interface. *Environmental science & technology*
501 **2010,** *44*, (22), 8491-8496.
502 20. Görn, M. G.; Bolanz, R. M.; Parry, S.; Göttlicher, J.; Steininger, R.; Majzlan, J.,
503 Incorporation of Mo^{6+} in ferrihydrite, goethite, and hematite. *Clays and Clay Minerals* **2021,**
504 *69*, (2), 1-17.
505 21. Brinza, L.; Benning, L. G.; Statham, P. J., Adsorption studies of Mo and V onto
506 ferrihydrite. *Mineralogical Magazine* **2008,** *72*, (1), 385-388.
507 22. Brinza, L.; Vu, H. P.; Shaw, S.; Mosselmans, J. F. W.; Benning, L. G., Effect of Mo
508 and V on the hydrothermal crystallization of hematite from ferrihydrite: An in situ energy
509 dispersive X-ray diffraction and X-ray absorption spectroscopy study. *Crystal Growth &*
510 *Design* **2015,** *15*, (10), 4768-4780.
511 23. Gustafsson, J. P., Modelling molybdate and tungstate adsorption to ferrihydrite.
512 *Chemical geology* **2003,** *200*, (1-2), 105-115.

24. Das, S.; Essilfie-Dughan, J.; Hendry, M. J., Sequestration of molybdate during transformation of 2-line ferrihydrite under alkaline conditions. *Applied geochemistry* **2016,** *73*, 70-80.
25. Wang, Z.; Peacock, C.; Kwon, K. D.; Gu, X.; Feng, X.; Li, W., Site-specific isotope fractionation during Zn adsorption onto birnessite: Insights from X-ray absorption spectroscopy, density functional theory and surface complexation modeling. *Geochimica et Cosmochimica Acta* **2023,** *348*, 68-84.
26. Song, X.; Wang, P.; Van Zwieten, L.; Bolan, N.; Wang, H.; Li, X.; Cheng, K.; Yang, Y.; Wang, M.; Liu, T., Towards a better understanding of the role of Fe cycling in soil for carbon stabilization and degradation. *Carbon Research* **2022,** *1*, (1), 5.
27. Wang, Y.; Liu, Z.; Huang, W.; Lu, J.; Luo, S.; Czech, B.; Li, T.; Wang, H., Capture-reduction mechanism for promoting Cr (VI) removal by sulfidated microscale zerovalent iron/sulfur-doped graphene-like biochar composite. *Carbon Research* **2023,** *2*, (1), 11.
28. Gustafsson, J. P.; Tiberg, C., Molybdenum binding to soil constituents in acid soils: an XAS and modelling study. *Chemical Geology* **2015,** *417*, 279-288.
29. Wang, X.; Sherman, D. M., Molecular speciation of Mo (VI) on goethite and its implications for molybdenum and its isotopic cycle in ocean. *Geochimica et Cosmochimica Acta* **2021,** *313*, 116-132.
30. Schoepfer, V. A.; Lindsay, M. B., Repartitioning of co-precipitated Mo (VI) during Fe (II) and S (-II) driven ferrihydrite transformation. *Chemical Geology* **2022,** *610*, 121075.
31. Boland, D. D.; Collins, R. N.; Miller, C. J.; Glover, C. J.; Waite, T. D., Effect of solution and solid-phase conditions on the Fe (II)-accelerated transformation of ferrihydrite to lepidocrocite and goethite. *Environmental science & technology* **2014,** *48*, (10), 5477-5485.
32. Zhu, M.; Frandsen, C.; Wallace, A. F.; Legg, B.; Khalid, S.; Zhang, H.; Mørup, S.; Banfield, J. F.; Waychunas, G. A., Precipitation pathways for ferrihydrite formation in acidic solutions. *Geochimica et Cosmochimica Acta* **2016,** *172*, 247-264.
33. Liu, J.; Sheng, A.; Li, X.; Arai, Y.; Ding, Y.; Nie, M.; Yan, M.; Rosso, K. M., Understanding the importance of labile Fe (III) during Fe (II)-catalyzed transformation of metastable iron oxyhydroxides. *Environmental Science & Technology* **2022,** *56*, (6), 3801-3811.
34. Liu, Y.; Ding, Y.; Sheng, A.; Li, X.; Chen, J.; Arai, Y.; Liu, J., Fe (II)-Catalyzed Transformation of Ferrihydrite with Different Degrees of Crystallinity. *Environmental Science & Technology* **2023,** *57*, (17), 6934-6943.
35. Xu, F.; Liu, Y.; Liu, C., A generalized-rate model for describing and scaling redox kinetics in sediments containing variable redox-reactive materials. *Environmental science & technology* **2018,** *52*, (9), 5268-5276.
36. Zhang, X.; Jia, Q.; Deng, J.; Wu, F.; Huang, L.-Z., Interaction between green rust and tribromophenol under anoxic, oxic and anoxic-to-oxic conditions: Adsorption, desorption and oxidative degradation. *Water Research* **2022,** *217*, 118398.
37. Hansel, C. M.; Benner, S. G.; Fendorf, S., Competing Fe (II)-induced mineralization pathways of ferrihydrite. *Environmental Science & Technology* **2005,** *39*, (18), 7147-7153.
38. Yee, N.; Shaw, S.; Benning, L. G.; Nguyen, T. H., The rate of ferrihydrite transformation to goethite via the Fe (II) pathway. *American Mineralogist* **2006,** *91*, (1), 92-96.
39. Lovley, D. R., Dissimilatory metal reduction. *Annual review of microbiology* **1993,** *47*, (1), 263-290.
40. Caccavo Jr, F.; Lonergan, D. J.; Lovley, D. R.; Davis, M.; Stolz, J. F.; McInerney, M. J., Geobacter sulfurreducens sp. nov., a hydrogen-and acetate-oxidizing dissimilatory metal-reducing microorganism. *Applied and environmental microbiology* **1994,** *60*, (10), 3752-3759.

41. Ortiz-Bernad, I.; Anderson, R. T.; Vrionis, H. A.; Lovley, D. R., Vanadium respiration by Geobacter metallireducens: novel strategy for in situ removal of vanadium from groundwater. *Applied and Environmental microbiology* **2004,** *70*, (5), 3091-3095.
42. Lloyd, J. R.; Leang, C.; Myerson, A. L. H.; Coppi, M. V.; Cuifo, S.; Methe, B.; Sandler, S. J.; Lovley, D. R., Biochemical and genetic characterization of PpcA, a periplasmic c-type cytochrome in Geobacter sulfurreducens. *Biochemical Journal* **2003,** *369*, (1), 153-161.
43. Carpentier, W.; Sandra, K.; De Smet, I.; Brige, A.; De Smet, L.; Van Beeumen, J., Microbial reduction and precipitation of vanadium by Shewanella oneidensis. *Applied and Environmental Microbiology* **2003,** *69*, (6), 3636-3639.
44. Byrne, J.; Telling, N.; Coker, V.; Pattrick, R.; Van Der Laan, G.; Arenholz, E.; Tuna, F.; Lloyd, J., Control of nanoparticle size, reactivity and magnetic properties during the bioproduction of magnetite by Geobacter sulfurreducens. *Nanotechnology* **2011,** *22*, (45), 455709.
45. Xie, J.; Coker, V. S.; O'Driscoll, B.; Cai, R.; Haigh, S. J.; Lloyd, J. R., Microbial reduction of antimony (V)-bearing ferrihydrite by Geobacter sulfurreducens. *Applied and Environmental Microbiology* **2023,** *89*, (3), e02175-22.
46. Coker, V.; Gault, A.; Pearce, C.; Van der Laan, G.; Telling, N.; Charnock, J.; Polya, D.; Lloyd, J., XAS and XMCD evidence for species-dependent partitioning of arsenic during microbial reduction of ferrihydrite to magnetite. *Environmental science & technology* **2006,** *40*, (24), 7745-7750.
47. Cutting, R. S.; Coker, V. S.; Telling, N. D.; Kimber, R. L.; Van Der Laan, G.; Pattrick, R. A.; Vaughan, D. J.; Arenholz, E.; Lloyd, J. R., Microbial reduction of arsenic-doped schwertmannite by Geobacter sulfurreducens. *Environmental science & technology* **2012,** *46*, (22), 12591-12599.
48. Xiu, W.; Yuan, W.; Polya, D. A.; Guo, H.; Lloyd, J. R., A critical review of abiotic and microbially-mediated chemical reduction rates of Fe (III)(oxyhydr) oxides using a reactivity model. *Applied Geochemistry* **2021,** *126*, 104895.
49. Coker, V. S.; van der Laan, G.; Telling, N. D.; Lloyd, J. R.; Byrne, J. M.; Arenholz, E.; Pattrick, R. A. D., Bacterial production of vanadium ferrite spinel (Fe,V)3O4 nanoparticles. *Mineralogical Magazine* **2020,** *84*, (4), 554-562.
50. Lovley, D. R.; Phillips, E. J., Organic matter mineralization with reduction of ferric iron in anaerobic sediments. *Applied and environmental microbiology* **1986,** *51*, (4), 683-689.
51. Shukor, M.; Rahman, M.; Shamaan, N. A.; Syed, M., Reduction of molybdate to molybdenum blue by Enterobacter sp. strain Dr. Y13. *Journal of Basic Microbiology* **2009,** *49*, (S1), S43-S54.
52. Newsome, L.; Morris, K.; Shaw, S.; Trivedi, D.; Lloyd, J. R., The stability of microbially reduced U (IV); impact of residual electron donor and sediment ageing. *Chemical Geology* **2015,** *409*, 125-135.
53. Lovley, D. R.; Phillips, E. J., Rapid assay for microbially reducible ferric iron in aquatic sediments. *Applied and Environmental Microbiology* **1987,** *53*, (7), 1536-1540.
54. Xie, J.; Zhao, Z.; Coker, V. S.; O'Driscoll, B.; Cai, R.; Haigh, S. J.; Holmes, S. M.; Lloyd, J. R., Bioproduction of cerium-bearing magnetite and application to improve carbon-black supported platinum catalysts. *Journal of Nanobiotechnology* **2024,** *22*, (1), 203.
55. Scherrer, P., Estimation of the size and internal structure of colloidal particles by means of röntgen. *Nachr. Ges. Wiss. Göttingen* **1918,** *2*, 96-100.
56. Holzwarth, U.; Gibson, N., The Scherrer equation versus the'Debye-Scherrer equation'. *Nature nanotechnology* **2011,** *6*, (9), 534-534.
57. Kudrin, A., The solubility of tugarinovite MoO2 in aqueous solutions at elevated temperatures. *Geochemistry International* **1985,** *22*, (9), 126-138.

58. Saha, P.; Anderson, A. J.; Lee, T.; Klemm, M., The Solubility of Tugarinovite (MoO 2) in H 2 O at Elevated Temperatures and Pressures. *Geofluids* **2017,** *2017*.
59. Wang, X.; Liu, Y.; Zeng, J.; Peng, C.; Wang, R., MoO 2/C hollow nanospheres synthesized by solvothermal method as anode material for lithium-ion batteries. *Ionics* **2019,** *25*, 437-445.
60. Lima, F. A.; Bjornsson, R.; Weyhermüller, T.; Chandrasekaran, P.; Glatzel, P.; Neese, F.; DeBeer, S., High-resolution molybdenum K-edge X-ray absorption spectroscopy analyzed with time-dependent density functional theory. *Physical Chemistry Chemical Physics* **2013,** *15*, (48), 20911-20920.
61. Coker, V. S.; Pearce, C. I.; Lang, C.; van der Laan, G.; Pattrick, R. A.; Telling, N. D.; Schüler, D.; Arenholz, E.; Lloyd, J. R., Cation site occupancy of biogenic magnetite compared to polygenic ferrite spinels determined by X-ray magnetic circular dichroism. *European Journal of Mineralogy* **2007,** *19*, (5), 707-716.
62. Hao, H.; Li, L.; Yuan, Z.; Patra, P.; Somasundaran, P., Adsorption differences of sodium oleate on siderite and hematite. *Minerals Engineering* **2019,** *137*, 10-18.
63. Wang, X.; Zhu, M.; Koopal, L. K.; Li, W.; Xu, W.; Liu, F.; Zhang, J.; Liu, Q.; Feng, X.; Sparks, D. L., Effects of crystallite size on the structure and magnetism of ferrihydrite. *Environmental Science: Nano* **2016,** *3*, (1), 190-202.
64. Hochella Jr, M. F.; Lower, S. K.; Maurice, P. A.; Penn, R. L.; Sahai, N.; Sparks, D. L.; Twining, B. S., Nanominerals, mineral nanoparticles, and earth systems. *science* **2008,** *319*, (5870), 1631-1635.
65. Das, S.; Hendry, M. J.; Essilfie-Dughan, J., Adsorption of selenate onto ferrihydrite, goethite, and lepidocrocite under neutral pH conditions. *Applied geochemistry* **2013,** *28*, 185-193.
66. Wang, Y.; Wang, J.; Li, P.; Qin, H.; Liang, J.; Fan, Q., The adsorption of U (VI) on magnetite, ferrihydrite and goethite. *Environmental Technology & Innovation* **2021,** *23*, 101615.
67. Marsac, R.; Pasturel, M.; Hanna, K., Reduction kinetics of nitroaromatic compounds by titanium-substituted magnetite. *The Journal of Physical Chemistry C* **2017,** *121*, (21), 11399-11406.
68. Klausen, J.; Troeber, S. P.; Haderlein, S. B.; Schwarzenbach, R. P., Reduction of substituted nitrobenzenes by Fe (II) in aqueous mineral suspensions. *Environmental science & technology* **1995,** *29*, (9), 2396-2404.
69. Gorski, C. A.; Scherer, M. M., Influence of magnetite stoichiometry on FeII uptake and nitrobenzene reduction. *Environmental science & technology* **2009,** *43*, (10), 3675-3680.
70. Li, Y.; Wei, G.; Liang, X.; Zhang, C.; Zhu, J.; Arai, Y., Metal substitution-induced reducing capacity of magnetite coupled with aqueous Fe (II). *ACS Earth and Space Chemistry* **2020,** *4*, (6), 905-911.
71. Kim, W.; Suh, C.-Y.; Cho, S.-W.; Roh, K.-M.; Kwon, H.; Song, K.; Shon, I.-J., A new method for the identification and quantification of magnetite–maghemite mixture using conventional X-ray diffraction technique. *Talanta* **2012,** *94*, 348-352.
72. Vermeire, M.-L.; Bonneville, S.; Stenuit, B.; Delvaux, B.; Cornélis, J.-T., Is microbial reduction of Fe (III) in podzolic soils influencing C release? *Geoderma* **2019,** *340*, 1-10.